JOURNAL OF GUIDANCE, CONTROL, AND DYNAMICS
Vol. 30, No. 3, May–June 2007

Autonomous Interplanetary Orbit Determination Using Satellite-to-Satellite Tracking

Keric Hill* and George H. Born†
University of Colorado, Boulder, Colorado 80309

DOI: 10.2514/1.24574

A new method of interplanetary orbit determination is described that uses only scalar satellite-to-satellite observations such as crosslink range to estimate the orbits of all of the participating spacecraft simultaneously. This method, called *liaison navigation*, does not work in the two-body problem or for constellations in low Earth orbits in which two-body dynamics dominate. If the constellation is strongly affected by a third body such as the moon, the gravitational effect of the third body can make all of the spacecraft states observable. In the three-body problem, spacecraft in the vicinity of the L_1 and L_2 Lagrange points experience significant accelerations due to both of the primary bodies, and these are ideal locations for investigating the feasibility of liaison navigation. Covariance analysis is used to estimate the accuracy of liaison navigation for spacecraft in Earth–moon and sun–Earth halo orbits generated in the circular restricted three-body problem. With only data noise, the estimation accuracy for the spacecraft positions in some configurations is excellent. In addition, a range bias is successfully estimated, along with the satellite states. Principles of constellation design that lead to more accurate liaison navigation estimates are described, along with techniques for reducing the fit-span length.

I. Introduction

MOST observations used to determine the orbits of interplanetary spacecraft are generated using Earth-based tracking sensors. Autonomous orbit determination is conducted using only the equipment aboard orbiting spacecraft. Remote spacecraft that can autonomously determine their positions are less reliant on Earth-based trackers such as the Deep Space Network (DSN). Several different methods of autonomous orbit determination have been proposed using different measurement types [1–7]. Some of these autonomous techniques rely on sensing the direction vector to a large body. The direction vector to the Earth may be estimated by sensing the Earth's limb or the Earth's magnetic field. Other sensed objects could be the sun or the moon. Star sensors are used to determine attitude information and provide the vector direction to the sensed object in the inertial frame. Crosslink range has been proposed as a method of increasing orbit determination accuracy or maintaining a navigation solution for a constellation for a limited time. Some studies [8,9] have suggested using crosslink range, attitude information, and an optical tracker to find the vector to another satellite and determine the orbits autonomously. Another study suggested using only optical tracking and attitude information to find the direction vector between the two spacecraft and determine both orbits [10].

This study will focus on autonomous navigation using only scalar satellite-to-satellite tracking (SST) observations such as crosslink range. The goal is to determine the combined satellite state vector without any supplemental ground tracking. SST only provides information on the relative motion of two or more spacecraft and is normally used in conjunction with Earth-based tracking to obtain information on the absolute position. For example, one spacecraft can be tracked from the ground while it tracks a second satellite. Combining the observations, one can successfully estimate the orbits of both satellites. This method is currently used to determine the orbits of spacecraft in low Earth orbit (LEO) with the tracking and data relay satellite system (TDRSS) and the global positioning system (GPS). However, in the two-body problem, SST cannot be used alone to estimate the absolute positions of the spacecraft involved. That is because in the two-body problem, SST only provides information on the size, shape, relative orientation of the orbits, and the spacecraft positions along the orbits.

Suppose an orbit exists with a unique size, shape, and absolute orientation. If a spacecraft in that orbit generates SST observations with respect to a second spacecraft, those measurements can be used to determine the size and shape of the unique orbit. Because there is only one orbit with that size and shape, the absolute orientation of that orbit is not ambiguous. The SST measurements also provide information on the relative orientation of the second trajectory, and so the absolute position of the second spacecraft would also be known. We propose a new method of orbit determination called linked, autonomous, interplanetary satellite orbit navigation (LIAISON) [11], hereafter referred to as liaison navigation. Liaison navigation means using SST observations to determine the relative and absolute orbits of two or more spacecraft when at least one of them is in an orbit with a unique size, shape, and orientation.

II. Unique Trajectories

A trajectory is unique when there is only one set of initial conditions that will result in a trajectory of that size and shape. To define what is meant by trajectories having the same size and shape, suppose that in an inertial frame, there are two spacecraft trajectories that will be called X_1 and X_2. The orbit state of X_i at time t would be

$$X_i(t) = [\, x_i(t) \quad y_i(t) \quad z_i(t) \quad \dot{x}_i(t) \quad \dot{y}_i(t) \quad \dot{z}_i(t) \,] \tag{1}$$

The two trajectories have the same size and shape if a constant 3×3 rotation θ and a constant 3×1 translation Δr can be found, such that

$$X_2(t) = \begin{bmatrix} \theta & [\emptyset]_{3\times3} \\ [\emptyset]_{3\times3} & \theta \end{bmatrix} X_1(t) + \begin{bmatrix} \Delta r \\ [\emptyset]_{3\times1} \end{bmatrix} \tag{2}$$

for all times t. For a trajectory with a unique size and shape, a rotation and translation does not exist that will make it equivalent to any other trajectory. To understand the circumstances under which a unique trajectory can exist, assume that the accelerations experienced by a spacecraft depend solely on its position and time. The equations of motion for the spacecraft in an inertial frame can be written

Received 5 May 2006; revision received 7 December 2006; accepted for publication 11 December 2006.

*Graduate Research Assistant, Colorado Center for Astrodynamics Research, Campus Box 429. Member AIAA.

†Director, Colorado Center for Astrodynamics Research, Campus Box 431. Fellow AIAA.

$$\ddot{\boldsymbol{r}} = \boldsymbol{f}(\boldsymbol{r}, t) \tag{3}$$

The characteristics of the acceleration function $\boldsymbol{f}(\boldsymbol{r}, t)$ determine whether a unique trajectory exists. A unique trajectory cannot exist if $\boldsymbol{f}(\boldsymbol{r}, t)$ and its time derivatives are symmetric. A function such as $\boldsymbol{f}(\boldsymbol{r}, t)$ is symmetric if a 3×3 rotation ϕ can be found, such that

$$\boldsymbol{f}(\boldsymbol{r}, t) = \phi \boldsymbol{f}(\boldsymbol{r}, t) \tag{4}$$

The following examples illustrate several acceleration functions and their symmetry.

A. Example 1: Two-Body Problem

In the two-body problem, a vector field of the resulting acceleration function $\boldsymbol{f}(\boldsymbol{r}, t)$ is symmetric about the center of the primary body. In this model, suppose a spacecraft is in orbit around the primary body and the initial position of the spacecraft is $\boldsymbol{r}_0 = [x_0 \quad y_0 \quad z_0]^T$. Because of the symmetry in the acceleration function, there can be an infinite number of orbits of the same size and shape. The initial positions of these similar orbits all lie on a sphere centered on the primary body with radius $\|\boldsymbol{r}_0\|$. If there were two spacecraft in orbit around the primary, SST observations could be taken between the two spacecraft and these observations could be used to estimate the size, shape, and relative orientation of the two orbits. However, the absolute orientation of the trajectories could not be estimated. Any rotation about the center of mass of the primary, if the same rotation were applied to both the position and velocity portions of the initial conditions of both orbits, would generate a new pair of orbits that could exist using the same acceleration function. They would have the same shape, size, and relative orientation and would result in exactly the same SST observations. The three state parameters required to describe the absolute orientation of the two orbits cannot be estimated from the SST observations alone. Thus, out of a total of 12 state parameters required to describe the absolute positions and velocities of the two spacecraft, only nine can be estimated with SST. Liu and Liu [12] showed that it is possible, except in some special cases, to estimate the semimajor axis, eccentricity, and true anomaly

$$\{a_1, \quad a_2, \quad e_1, \quad e_2, \quad \nu_1, \quad \nu_2\}$$

of two satellites in the two-body problem using only SST. The subscripts indicate the satellite number. These are the Keplerian orbital elements related to the size and shape of the orbits and the location of the satellite relative to periapsis. Difficulties arise when attempting to estimate the Keplerian elements that are related to orientation, such as the inclination, the longitude of the ascending node, and the argument of perigee:

$$\{i_1, \quad i_2, \quad \Omega_1, \quad \Omega_2, \quad \omega_1, \quad \omega_2\}$$

They concluded that this difficulty could be avoided by fixing the longitude of the ascending node and the inclination for both satellites and only estimating the argument of perigee. Fixing these four state parameters resulted in an observable state in the orbit determination problem. However, it should be possible to estimate three orientation parameters instead of just two. When projected onto the surface of a sphere, the orbits appear as two great circles with two intersections. Figure 1 is a spherical triangle showing that the relative orientation of the periapses of the two orbits can be described with three state parameters: d is the angle between the two orbit planes at their intersection on the sphere; c_1 describes the angular distance along the first orbit from the periapse to one of the two intersections of the orbits (this angle is positive in the direction of orbital motion); and c_2 describes the angular distance along the second orbit from the periapse to the same intersection of the orbits. The Keplerian orientation elements can be varied with the constraint that d, c_1, and c_2 remain constant without creating any change in the SST observations.

Figure 1 also shows how the parameters d, c_1, and c_2 can be described in terms of the Keplerian elements. This is done using spherical trigonometry and the equations for all three relative

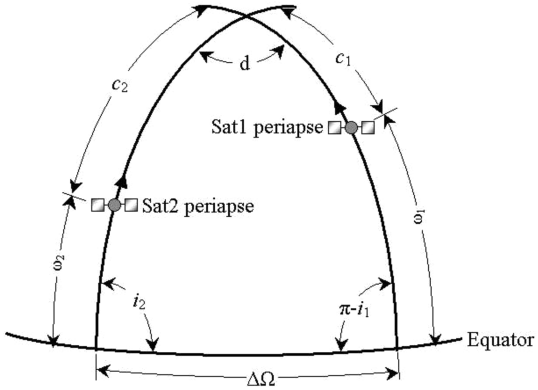

Fig. 1 Spherical triangle representing the relative orientation of two orbits projected onto a sphere.

orientation parameters in terms of the Keplerian orientation parameters are

$$d = \cos^{-1}[\cos(i_1)\cos(i_2) + \sin(i_1)\sin(i_2)\cos(\Delta\Omega)] \tag{5}$$

$$c_1 = \tan^{-1}\left[\frac{\sin(\Delta\Omega)}{\sin(i_1)\cot(i_2) - \cos(i_1)\cos(\Delta\Omega)}\right] - \omega_1 \tag{6}$$

$$c_2 = \tan^{-1}\left[\frac{\sin(\Delta\Omega)}{-\sin(i_2)\cot(i_1) + \cos(i_2)\cos(\Delta\Omega)}\right] - \omega_2 \tag{7}$$

Because d, c_1, and c_2 represent the relative orientation, it should be possible to estimate all three using only SST. To test this, the observability of the state vector with nine parameters was verified with covariance analysis using the batch processor, a least-squares method [13]. The details of that method are summarized in the Appendix. Using the batch processor, the information matrix Λ is computed. The entire state is observable only if Λ is positive definite and has a condition number less than 10^{16}. The variance–covariance matrix P is the inverse of the information matrix and will be useful for computing error metrics.

Trajectories were simulated for two spacecraft in various low Earth orbits using a two-body propagator. These ephemerides were propagated over 6-h fit spans. Crosslink range observations were generated every 20 s. The standard deviation of the noise on the range measurements was 1 m. After accumulating the information matrix for each set of orbits, it was found that the entire nine-parameter state was observable using only crosslink range. In all of these cases, the estimates for d, c_1, and c_2 had variances of less than a thousandth of a degree. However, it should be noted that there are exceptional cases in which the nine-parameter state would not be observable, such as when one spacecraft is following the other in the same circular orbit.

Next, the parameters d, c_1, and c_2 were removed from the state vector and replaced with different combinations of three of the Keplerian orientation parameters. Equations (5–7) were substituted into Eq. (A4) to get the range in terms of the Keplerian orientation elements. Using the same two-body trajectories mentioned previously, orbit determination simulations showed that none of the combinations of three Keplerian orientation elements could be simultaneously observed using only SST. These results lead to the conclusion that there seems to be inherent limitations in the Keplerian orientation elements that make it impossible to estimate three simultaneously using only SST in the two-body problem.

Liu and Liu [12] were able to create an observable state by fixing four of the unknowns (i_1, i_2, Ω_1, and Ω_2) and solving for the other two (ω_1 and ω_2). To see if there were other combinations of two Keplerian orientation parameters that could be observed, the observability tests were repeated. This time, the state vector was defined so that it only included two of the Keplerian orientation

parameters in different combinations. The results of that study show that it is possible to solve for any combination of two orientation-type Keplerian elements except for Ω_1 and Ω_2. This is because Ω_1 and Ω_2 only appear in the equations in difference form $\Delta\Omega$, and so they cannot be estimated simultaneously.

B. Example 2: Two-Body Problem with J_2

Suppose that the gravity model for the primary body in the two-body problem is expanded to include the J_2 term representing the equatorial bulge. Both Psiaki [8] and Yim et al. [10] mentioned that the effects of J_2 make the intersatellite orbit determination problem more observable. With J_2, the function $\boldsymbol{f}(\boldsymbol{r}, t)$ is symmetric about the z axis of the primary body and the equatorial plane. If the initial position of a spacecraft is $\boldsymbol{r}_0 = [x_0 \quad y_0 \quad z_0]^T$, then there can be orbits of the same size and shape, beginning anywhere on two circles described by the following equations:

$$x^2 + y^2 = x_0^2 + y_0^2, \qquad z = \pm z_0 \tag{8}$$

The angle describing the position of the spacecraft on the circle and the sign of the z component are not observable with SST. Thus, if there were two spacecraft orbiting the Earth in this model, SST observations could only be used to observe 10 of the 12 state parameters.

C. Example 3: Three-Body Problem

For a three-body problem, suppose an inertial coordinate frame has its origin at the center of mass of the system, with the x axis initially extending through both primaries. The two primaries orbit about their mutual center of mass, or barycenter. At any one instant, the function $\boldsymbol{f}(\boldsymbol{r}, t)$ is symmetric about the line joining the two primaries. However, because the two primaries are moving about the barycenter in an inertial frame, the function $(d/dt)\boldsymbol{f}(\boldsymbol{r}, t)$ provides asymmetry in the direction of the motion of the primaries. The only dimension without asymmetry in either $\boldsymbol{f}(\boldsymbol{r}, t)$ or $(d/dt)\boldsymbol{f}(\boldsymbol{r}, t)$ would be the orbit plane of the primaries. Trajectories in that three-body problem are not truly unique, because each is part of a symmetric pair. For each trajectory that exists in the three-body problem, another valid trajectory can be found by changing the sign on the z components of position and velocity. In the case of halo orbits, these groups of symmetric orbits are called the northern and southern halos. However, if the symmetric orbit states are sufficiently different, they can be said to be "locally unique."

For two spacecraft using SST in the three-body problem, the sign of the z components, or the components of the position and velocity perpendicular to the orbit plane of the primaries, cannot be estimated, and so only the remaining 11 of the 12 state parameters are estimable. If the two symmetric orbit states are sufficiently different, a priori knowledge of the spacecraft's state could be used to select the proper sign of the z components of the state. Then all 12 of the state parameters for the two satellites could be simultaneously estimated.

In other words, SST alone can be used to determine the orbits of a constellation of spacecraft if there is a strong gravitational acceleration due to at least two primary bodies. The influence of the gravity of the second primary body provides information on the orientation of the constellation with respect to the two primary bodies. Because the gravitational acceleration is larger when a spacecraft is closer to a body, a constellation with one spacecraft in a low orbit about one primary and another spacecraft in a low orbit about the second primary would result in the best liaison navigation accuracy. That is because the constellation is very strongly influenced by both primaries. An example of that would be an Earth-orbiting satellite tracking a spacecraft in lunar orbit. However, it would be desirable to have a constellation that is not so far apart. The focus of Sec. III will be to find regions in which the gravitational attraction of both primaries is strongly felt.

III. Strength of the Asymmetry

Although unique orbits are possible with the asymmetry in the third-body acceleration function, observation noise and uncertainties in the spacecraft force model could obliterate the effects of this asymmetric acceleration on the resulting orbital path. For practical purposes, the effect of the asymmetric acceleration on the spacecraft trajectory must be significantly greater than the observation noise and the effects due to unmodeled accelerations.

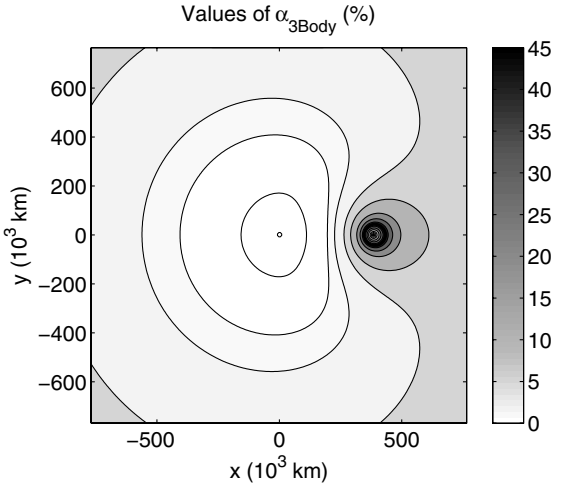

Fig. 2 Map of α for acceleration due to the third body in the Earth–moon system.

One way of evaluating the strength of these asymmetric accelerations is to look at the magnitude of the acceleration caused by the perturbations compared with the sum of the magnitudes of all of the accelerations at any one location. The parameter α_j will be used to quantify the relative strength of perturbation j:

$$\alpha_j(x, y, z) = \frac{|\ddot{\boldsymbol{r}}_j(x, y, z)|}{\sum_{i=1}^{n} |\ddot{\boldsymbol{r}}_i(x, y, z)|} \tag{9}$$

If there are n sources of acceleration acting on the spacecraft, $\ddot{\boldsymbol{r}}_i(x, y, z)$ represents acceleration i at location (x, y, z), with $i = 1 \ldots n$. The larger the value of $\alpha_j(x, y, z)$ for an asymmetric acceleration, the more likely that a spacecraft at location (x, y, z) would be able to use liaison navigation. Two-dimensional maps of α were created for a simplified Earth-centered system. The coordinate axes were Earth-centered-inertial, with the Earth's gravity modeled as a point mass. The maps were created to depict a single instant in time. At that instant, the positive x axis extends through the moon's point mass. The sun lies along the positive y axis, which is perpendicular to the x axis. Accelerations due to drag, J_2, solar radiation pressure (SRP), Earth's point mass, and the perturbations

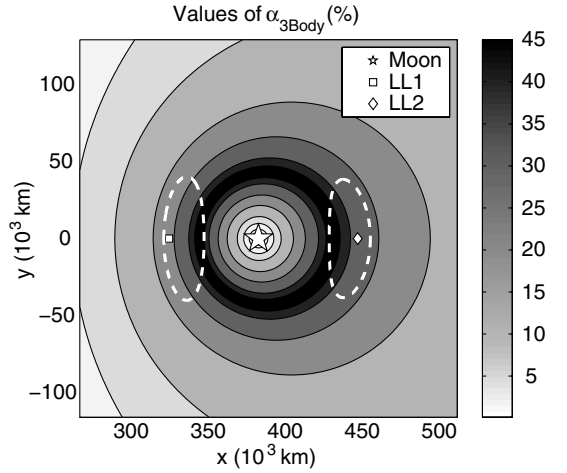

Fig. 3 Map of α near the moon for acceleration due to the third body in the Earth–moon system. The positions of the lunar L_1 and L_2 Lagrange points are shown, along with a halo orbit around each.

due to the moon and sun were included in the calculations and computed using equations from Tapley, et al. [13].

Figure 2 shows a map of α for the third-body perturbation. Note that within the sphere of influence of the moon, the Earth is considered the third body. Remember that the purpose of this figure is to find a region in which the gravity of both primary bodies is felt strongly. Figure 2 shows that the third-body perturbation is very strong in a nearly spherical shell around the moon, for which α reaches a maximum of about 45%. Figure 3 shows that halo orbits around the lunar Lagrange points L_1 and L_2 stay within regions of high α for their entire periods.

IV. Circular Restricted Three-Body Problem

Figure 3 shows that three-body gravity, especially in libration point orbits, is the most likely perturbation to enable successful liaison navigation for close constellations. Simulations of SST measurements generated between two spacecraft in Earth–moon libration point orbits were used to check that liaison navigation could completely observe both orbits. The simplest libration point orbits to create are the periodic halo [14] orbits in the circular restricted three-body problem [15] (CRTBP). In the CRTBP, there are two primary bodies with point masses in coplanar circular orbits about their mutual barycenter. A spacecraft with infinitesimal mass is gravitationally attracted by both primaries. The more massive body is labeled P_1 and the less massive is P_2. The coordinate frame has its origin at the barycenter and rotates with the two bodies so that P_1 and P_2 are always on the x axis, with the positive x direction going from P_1 to P_2. The positive y axis is parallel to the velocity vector of P_2 and the z axis is perpendicular to the plane of the primary orbits. The mass is nondimensionalized so that the mass of P_2 is μ and the mass of P_1 is $1-\mu$; μ is computed with the following equation:

$$\mu = \frac{\mu_{P2}}{\mu_{P1} + \mu_{P2}} \tag{10}$$

where μ_{P1} and μ_{P2} are the masses or gravitational parameters of the two primaries. The distance between the two primaries is one length unit (LU), with P_1 at $-\mu$ on the x axis and P_2 at $1-\mu$ on the x axis. The time unit (TU) is defined such that the orbit period of the primaries is 2π TU.

The equations of motion for the nondimensionalized CRTBP are

$$\ddot{x} - 2\dot{y} = x - (1-\mu)\frac{x+\mu}{r_1^3} - \mu\frac{x+\mu-1}{r_2^3} \tag{11}$$

$$\ddot{y} + 2\dot{x} = \left(1 - \frac{1-\mu}{r_1^3} - \frac{\mu}{r_2^3}\right)y \tag{12}$$

$$\ddot{z} = \left(\frac{\mu-1}{r_1^3} - \frac{\mu}{r_2^3}\right)z \tag{13}$$

where

$$r_1 = \sqrt{(x+\mu)^2 + y^2 + z^2}, \qquad r_2 = \sqrt{(x+\mu-1)^2 + y^2 + z^2} \tag{14}$$

Five equilibrium points exist in the CRTBP when using a rotating coordinate frame. A spacecraft placed on an equilibrium point with zero velocity will remain at that equilibrium point indefinitely. These points are called Lagrange points or libration points. Three of the equilibrium points are on the x axis. L_3 is on the far side of the larger body, L_1 lies between the two bodies, and L_2 is on the far side of the smaller body. L_4 and L_5 are in the x–y plane and each forms an equilateral triangle with the two bodies.

Halo orbits were computed using the technique explained by Howell [16]. Families of halo orbits were generated around all three of the collinear Lagrange points in the Earth–moon system (LL_1, LL_2, and LL_3). For each family of halo orbits, a certain number were selected as test orbits and ephemeris files were generated. Figure 4 shows the representative distribution of the initial conditions in the LL_1 family.

A representative set of ephemerides for lunar and Earth orbits were also generated for testing, because only one of the spacecraft in a constellation must be near a libration orbit for liaison navigation to work. The Earth- and moon-centered orbits were propagated using the equations of motion for the three-body problem in the same rotating frame as the halo orbits.

Two spacecraft can be placed in these different orbits in many different combinations. When both spacecraft are in the same halo orbit, the constellation will be called $halo_2$. When the spacecraft are in different halo orbits, the constellation will be called halo–halo. When the spacecraft are in a halo and a moon- or Earth-centered orbit, the constellations will be called halo–moon or halo–Earth.

V. Liaison Navigation Test Methods

Observability tests were conducted using the equations in the Appendix, with some modifications. In the simulations, two spacecraft were placed in the test orbits in a systematic manner so that all of the $halo_2$, halo–halo, halo–moon, and halo–Earth constellations were examined. The two spacecraft tracked each other continuously, unless the Earth or the moon blocked the line-of-sight (LOS) vector. Range observations were generated from the ephemeris files every 0.001 time units, or about 375 s. The information matrix Λ was computed, and the covariance matrix was used to compute navigation error metrics. The range observations had an added white noise component with a standard deviation of 1 m.

In this study, the method used to compare the accuracy of orbit estimates was to propagate the batch covariance matrix over the entire fit span with the relation

$$P_i = \Phi(t_i, t_k) P_k \Phi^T(t_i, t_k) \tag{15}$$

where Φ, which is called the state transition matrix, was computed numerically by integrating the equation

$$\dot{\Phi}(t, t_k) = A(t)\Phi(t, t_k) \tag{16}$$

where

$$A(t) = \frac{\partial F(\boldsymbol{X}^*, t)}{\partial \boldsymbol{X}(t)}, \qquad \dot{\boldsymbol{X}} = F(\boldsymbol{X}, t)$$

and $\boldsymbol{X}^*$ is the reference solution, or the "best guess" orbit. Then the length of the largest axis of the 3-D, 3σ error ellipsoid for the spacecraft was computed. It will be called β_i at time t_i:

$$\beta_i = \max(\sqrt{\lambda_j}) \tag{17}$$

where λ_j for $j = 1, \ldots, 3$ are the eigenvalues of $[P_i]_{3\times 3}$. The average value of β_i over the entire data span will be called $\bar{\beta}$:

$$\bar{\beta} = \frac{\sum_{i=1}^{n} \beta_i}{n} \tag{18}$$

where there are n values of β_i in the fit span. If there are multiple satellites, the values of $\bar{\beta}$ for all of the satellites can be averaged to produce a metric called β_{ave} that gives an indication of the overall navigation accuracy for the constellation for those particular conditions.

With $halo_2$ constellations and various initial phase angles, the conventional Kalman filter was used to investigate how long it took to converge on a good solution with no process noise. After looking at these Kalman filter results for several different halo orbits, it was found that it took a little more than one halo orbit period for the solution to converge, regardless of the halo orbit period. This means that operationally, the halo orbits with a shorter period will lead to quicker convergence. In picking the fit span, it was decided to use 1.5

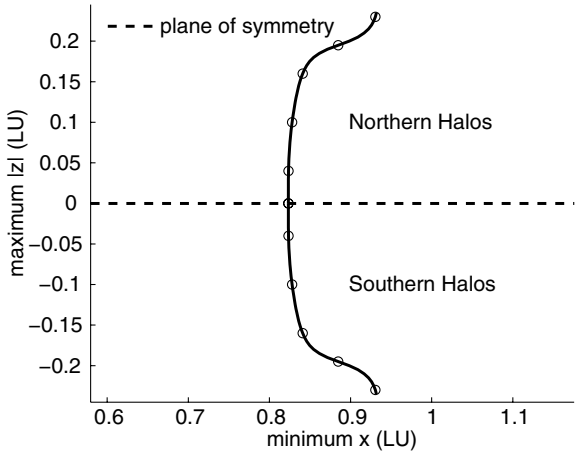

Fig. 4 Initial conditions for the LL_1 halo orbit family; circles indicate values used to generate ephemerides.

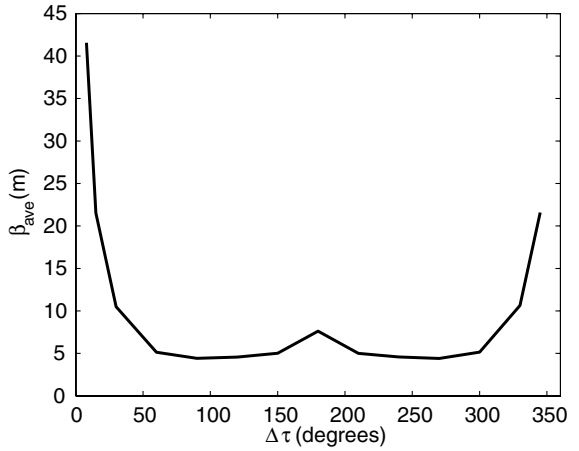

Fig. 6 Navigation accuracy for two spacecraft in the same halo orbit with varying separation in phase angle τ.

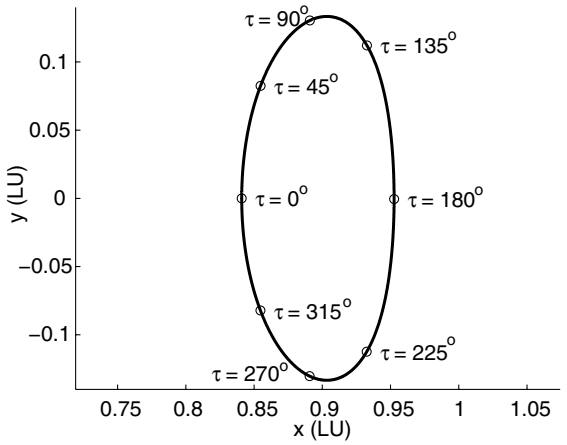

Fig. 5 Positions of various values of the phase angle τ on an LL_1 halo orbit projected onto the x–y plane.

halo orbit periods for all tests involving $halo_2$ and halo–halo constellations. In halo–Earth and halo–moon constellations, the integration time was shortened to 0.5 halo orbit periods.

When placing the spacecraft in halo orbits, it became convenient to define a phase angle τ, which is a nongeometric angle describing the positions of the spacecraft in the halos in a manner similar to mean anomaly, in that the phase angle has a constant time derivative. The phase angle is zero at the intersection of the halo orbit and the x–z plane, with the velocity in the positive y direction. The phase angle increases in the direction of the orbital motion and is defined as

$$\tau_i = [(t_i - t_0)/p]2\pi \tag{19}$$

where $(t_i - t_0)$ is the time past the x–z plane crossing (at $\tau = 0$) and p is the halo orbit period. Figure 5 shows some values of τ on a halo orbit that has been projected onto the x–y plane.

The value of the error metric β_{ave} varies with the separation of the two spacecraft in terms of phase angle, and so it became necessary to find one representative value of β_{ave} for each combination of two orbits. This metric will be called β_{con} and is used to rank the navigation accuracy of the different constellation geometries. β_{ave} metrics were generated using 15 different values of $\Delta\tau$ and three values of τ_1, for a total of 45 different runs for each combination of two orbits. The best value of β_{ave} that could be maintained indefinitely in time was selected as β_{con}. Because there is an infinite number of relative and absolute positions possible, the β_{con} metric is only an approximation. By observing the general behavior of the β_{ave} metric for many different cases and selecting the 45 runs properly, the error in this approximation was judged to be sufficiently small that β_{con} would be a useful metric for comparing constellations.

VI. Results in the Earth–Moon System

The results of the simulations showed that the initial position and velocity vectors of both spacecraft were observable for almost all constellations using only crosslink range. In other words, the condition number of the information matrix was less than 10^{16} for almost all cases. Among these observable cases, the covariances show that some of the best constellations had values of β_{con} that were less than 1 m, whereas the worst constellation geometries resulted in values of β_{con} in the thousands of kilometers. The results that follow give more insight into these vast differences in orbit determination accuracy and could aid a constellation designer in choosing orbits to minimize orbit determination error.

With both spacecraft starting at different phase angles in the same halo, the difference in phase angle, $\Delta\tau = \tau_2 - \tau_1$, remains constant. Figure 6 shows how the orbit determination accuracy varies with $\Delta\tau$.

Figure 6 shows that the orbit determination error goes up as the spacecraft get closer to each other, and the state becomes unobservable as they approach $\Delta\tau = 0$ deg. This is because the magnitude of the relative motion of the spacecraft decreases as the distance between them decreases. Thus, liaison navigation would not work for absolute positioning of spacecraft in close formations. That means there is a conflict between the need for large spacecraft separation and the desire for constellations without excessive link distances. However, it is not difficult to satisfy both conditions. Figure 6 shows that separating the spacecraft by as little as 60 deg of $\Delta\tau$ results in good orbit determination results.

Initial tests of $halo_2$ constellations at LL_1 showed that the navigation error was large for the halo orbits with very small z components. These orbits were the closest to the x–y plane, which is the orbit plane of the Earth and moon, or the plane of symmetry. Because these orbits are very close to the plane of symmetry, they are very nearly planar. Thus, the two spacecraft were very nearly in the same plane throughout the orbit, and there was very little out-of-plane component to the observations, making the out-of-plane component difficult to observe. Several more LL_1 halo orbits were integrated close to the x–y plane, and the values of β_{con} were separated into x, y, and z components and plotted in Fig. 7. For this plot, observations were computed at varying time intervals so that each $halo_2$ constellation would produce the same number of observations in 1.5 halo orbit periods. It shows that the out-of-plane component, which is the z component in this case, is very difficult to observe for the halo orbits near the plane of symmetry or with values of maximum $|z|$ near zero. It appears that the z component of the position is not well resolved until the value of maximum $|z|$ is at least 0.04 LU. In general, any constellations that are coplanar or nearly

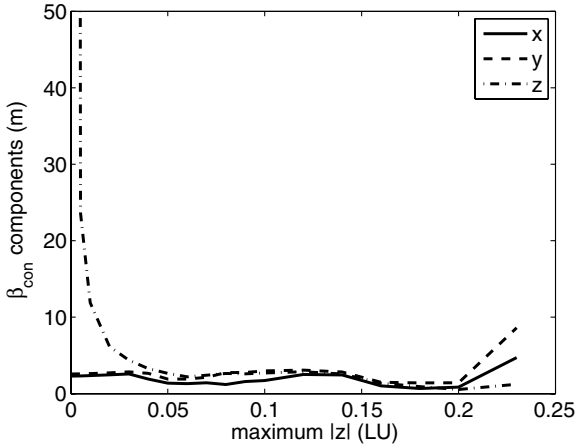

Fig. 7 β_{con} separated into x, y, and z components for LL_1 halo$_2$ constellations.

coplanar will suffer from this same problem. Also, the state is unobservable when $x_1 = x_2$, $y_1 = y_2$, and $z_1 = -z_2$.

The results from LL_2–halo$_2$ constellations follow a similar pattern to the LL_1 results shown in Fig. 7.

The LL_3 constellations had orbit determination errors that were around 10 times larger than the LL_1 and LL_2 constellations. This seems to agree with Fig. 2, which shows that the strength of the asymmetry of the third-body perturbation is weak at LL_3. In addition, the LL_3–Earth constellations had very poor observability. This is because most of the orbit dynamics at LL_3 are due to the Earth's gravity, not the moon's.

The orbit determination accuracy for the halo–moon constellations was similar to the LL_1 and LL_2 halo–halo accuracy, even though the fit span was only a third as long. It was also confirmed that liaison navigation works well when one spacecraft is in a lunar orbit and one is in an Earth orbit, although this might not have as much practical application due to the large link distances.

Next, using just a few select constellations, an error in the range measurements was introduced in the form of a range bias error with a standard deviation of 5 m. The range bias was added to the state to be estimated along with the positions and velocities of both spacecraft. The results showed that it is possible to estimate the range bias using only SST, but with an increase in the position and velocity errors.

A final run with the batch processor was meant to simulate, as closely as possible, the orbit accuracy attainable in a real operations environment. This run was performed using an LL_2 halo orbit and an eccentric, polar lunar orbit. In this run, the interval between observations was reduced to 0.0001 time units, or about 37.5 s. A range bias was included in the estimated state vector. The effect of an error in the force model was computed using the consider covariance technique outlined by Tapley et al. [13] Constant errors in the x, y, and z components of acceleration were modeled as three consider parameters for each satellite. The standard deviation for the error in the accelerations was set at 1×10^{-8} m/s^2. Two-h communication periods were separated by 2-h periods with no observations. The maximum range between the spacecraft was about 86,000 km. The results gave a $\bar{\beta}$ of 17.4 m for the satellite in the halo orbit and 2.4 m for the satellite in lunar orbit.

VII. Monte Carlo Analysis of the Covariance

To verify that the covariance matrices used were correct, a Monte Carlo analysis was conducted using the same halo–moon constellation mentioned in the last section. This time, the orbit states were actually estimated instead of only examining the covariances. Observations were processed every ~375 s, with 2-h blackout periods. A range bias was added to the state vector, and the fit span was 0.5 halo orbit periods long. The initial satellite states were perturbed by normally distributed random numbers with a standard deviation of 1×10^{-6} (about 384 m for position and 1 mm/s for velocity). The range bias was perturbed with a normally distributed random number with a standard deviation of 5 m. After converging on a solution, the estimated state was compared with the true state. This was done 1000 times. If the covariance matrix is realistic, the orbit error will be inside the 3-D, 2σ error ellipsoid for 73.9% of the runs. To find if the error is inside the 2σ error ellipsoid, the size of the error ellipsoid that intersects the orbit error vector is computed for each satellite. The size of the ellipsoid L has units of standard deviations σ and is computed as shown in Tapley, et al. [13]:

$$L^2_{\text{sat},i} = \delta \boldsymbol{r}_i^T P_i^{-1} \delta \boldsymbol{r}_i \tag{20}$$

where $\delta \boldsymbol{r}_i$ is the position error vector for spacecraft i, or the true state subtracted from the state estimate; and P_i is the 3×3 position covariance matrix for spacecraft i. For this halo–moon constellation, 74% of the values of $L_{\text{sat},1}$ and 73% of the values of $L_{\text{sat},2}$ were below 2σ. For the range bias covariance to be accurate, the range bias error should be less than 2σ for 95.4% of the runs. The range bias error was within 2σ for 98% of the runs.

A halo–halo constellation was also tested in the same way. The two spacecraft were both at LL_1, but in different halo orbits. For this constellation, 72% of the values of $L_{\text{sat},1}$, 71% of the values of $L_{\text{sat},2}$, and 97% of the range bias errors were below 2σ. For the halo–moon constellation, the covariance appears to be accurate, but the covariance is optimistic by a few percentage points for the halo–halo constellation. This is probably because the accuracy of the halo–halo orbit estimates was worse than for the halo–moon orbits, and the dynamics are so highly nonlinear in halo orbits that the linear approximation used to generate the state transition matrix results in a small error.

VIII. Improving Accuracy

It was mentioned that convergence using a Kalman filter required a fit span of about one halo orbit period. For a halo orbiter to perform a stationkeeping maneuver several times per orbit, a fit that spans less than the desired stationkeeping period would be needed. Other conditions may exist in which improved orbit determination accuracy is needed within a given fit span length.

As an example, Genesis was a recent mission to the sun–Earth libration points. The fit spans used for Genesis had to be about 60 days, or about one-third of a halo orbit period, so that stationkeeping maneuvers could be performed. The general characteristics of the Genesis science orbit [17], were used to generate a similar halo orbit in the CRTBP, with a period of about six months. Using two spacecraft in this CRTBP halo orbit, crosslink range observations were simulated for a 60-day fit. β_{con} was 774 km for the optimum $\Delta\tau$. This level of accuracy would not have been acceptable for Genesis, which had orbit determination requirements on the order of 10 km for position. The reason for the large error was that the fit span was too short for liaison navigation to converge properly. Improved orbit determination accuracy would be needed.

Decreasing the interval between observations, which increases their number, did not have a significant effect on the error metric, but adding an additional satellite was much more effective. With three satellites on the same halo orbit separated by 120 deg of phase angle, β_{con} was 690 m. Another effective way of achieving improved accuracy using liaison navigation would be to put one spacecraft in the sun–Earth halo orbit and the other into a very short-period orbit, such as an Earth orbit.

A number of tests were run using the Kalman filter with different types of constellations to test the speed of convergence. The time to convergence was judged visually without process noise. From the results of these tests, an approximate relationship between the number and placement of the spacecraft and the speed of convergence was generated. The results shown in Table 1 describe approximately how long it takes to converge on a solution using liaison navigation (in terms of halo orbit periods) based on the number of satellites in various constellations. Of course, actual results vary and should always be verified for any particular mission being planned.

Table 1 Approximate speed of convergence for liaison navigation with various constellation types

No. of halo spacecraft	No. of planetary spacecraft[a]	Convergence time in halo orbit periods
2	0	1
3	0	1/2
4	0	1/3
5	0	1/4
1	1	1/4
2	1	1/8

[a]An example of a planetary spacecraft in the Earth–moon system would be a lunar orbit with a period much shorter than the halo orbit.

From Table 1, it can be seen that the short-period planetary orbits lead to the fastest convergence for a specific number of spacecraft, or to the best orbit determination accuracy for a given fit span length. The shorter the planetary orbit period, the sooner the estimate for that orbit converged, whereas the halo orbit estimates always took longer.

IX. Conclusions

It was shown that asymmetry in the acceleration field can enable autonomous orbit determination using only SST. According to Merriam–Webster [18], liaison means "communication for mutual understanding," and so the name *liaison navigation* is appropriate because it is a method of intersatellite communication that achieves mutual understanding of their orbit states. Based on the simulations in this study, liaison navigation in lunar halo orbits not only appears possible, but also has the potential to be highly accurate.

When designing constellations for use in liaison navigation, the following principles apply:

1) The constellation should be strongly influenced by two primary bodies.

2) Constellation spacecraft should have relatively large separations.

3) The constellation orbits should not be coplanar or with separation purely in the z direction.

4) Constellation orbits with shorter periods lead to improved accuracy.

5) More spacecraft in the constellation leads to improved accuracy.

These simulations only included data noise and did not include perturbations to the CRTBP. However, simulations have been performed that include fourth-body gravitational affects, as well as SRP, with similar results [19]. Other simulations were performed for a low lunar orbiter and a halo orbiter at LL_2. With realistic modeling errors in the lunar gravity field, SRP, and maneuver execution, the 1σ position accuracy was 7 m for the low lunar orbiter and 80 m for the LL_2 halo orbiter [20]. If results like this could be attained in actual operation, the improved orbit accuracy for spacecraft in libration point orbits provided by liaison navigation would lead to a decrease in the ΔV needed for stationkeeping, because more accurate knowledge of the orbit leads to smaller stationkeeping budgets [21].

Using liaison navigation, a constellation of spacecraft in lunar halo orbits could be used as a communication relay for lunar orbiters and landers and as a tracking network to provide lunar surface positioning and orbit determination. This would be a significant asset in carrying out the President's vision for exploration of the moon, while reducing some of the burden on the DSN.

Appendix

In Sec. II, simulated crosslink range measurements were used to estimate the nine-parameter state vector

$$\boldsymbol{X} = [\,a_1 \quad e_1 \quad \nu_1 \quad a_2 \quad e_2 \quad \nu_2 \quad d \quad c_1 \quad c_2\,]^T \tag{A1}$$

in the two-body problem using the batch processor. The batch processor equations used were from Tapley, et al. [13] and are summarized here. The observations can be related to the state with the $\tilde{H}$ matrix, which is

$$\tilde{H}_i = \left[\frac{\partial G}{\partial \boldsymbol{X}}\right]_i^* \tag{A2}$$

where G is a function that computes observations $\boldsymbol{Y}_i$ from a state vector $\boldsymbol{X}_i$ at time i in the following way:

$$\boldsymbol{Y}_i = G(\boldsymbol{X}_i, t_i) + \epsilon_i \tag{A3}$$

where ϵ_i is the observation error. For this test, crosslink range ρ is the observation type, which can be written in terms of the Keplerian size and shape parameters and the relative orientation parameters defined in Eqs. (5–7):

$$\rho = \sqrt{r_1^2 + r_2^2 - 2r_1 r_2[\cos(c_1 - \nu_1)\cos(c_2 - \nu_2) + \sin(c_1 - \nu_1)\sin(c_2 - \nu_2)\cos(d)]} \tag{A4}$$

$$r_1 = \frac{a_1(1 - e_1^2)}{1 + e_1\cos(\nu_1)} \qquad r_2 = \frac{a_2(1 - e_2^2)}{1 + e_2\cos(\nu_2)} \tag{A5}$$

$\tilde{H}_i$ would then be of the form

$$\tilde{H}_i = \left[\frac{\partial\rho}{\partial a_1} \quad \frac{\partial\rho}{\partial e_1} \quad \frac{\partial\rho}{\partial \nu_1} \quad \frac{\partial\rho}{\partial a_2} \quad \frac{\partial\rho}{\partial e_2} \quad \frac{\partial\rho}{\partial \nu_2} \quad \frac{\partial\rho}{\partial d} \quad \frac{\partial\rho}{\partial c_1} \quad \frac{\partial\rho}{\partial c_2}\right]_i \tag{A6}$$

The $\tilde{H}_i$ matrix at time t may be mapped back to the initial epoch t_k with the state transition matrix Φ, which is described in Eq. (16). The result is the H_i matrix:

$$H_i = \tilde{H}_i\Phi(t_i, t_k) \tag{A7}$$

If there are ℓ observations, all of them can be combined into a vector, and all of the H_i matrices into a larger matrix, so that

$$H \equiv \begin{bmatrix} H_1 \\ \vdots \\ H_\ell \end{bmatrix} \tag{A8}$$

If it is assumed that the observation errors can be modeled as white noise, and the standard deviation in the observation noise is denoted σ_ρ, $W = 1/\sigma_\rho^2$ can be used to weight the observations, and the matrix $H^T WH$ can be accumulated one observation at a time:

$$H^T WH = \sum_{i=1}^{\ell} H_i^T WH_i \tag{A9}$$

$H^T WH$ is also called the information matrix Λ. The entire state is observable only if Λ is positive definite. The variance–covariance matrix is the inverse of the information matrix:

$$P = \Lambda^{-1} = \left(H^T WH + P_0^{-1}\right)^{-1} \tag{A10}$$

The covariance matrix can be used to compute the variances of errors in the state parameters, as well as the correlations between these errors. To check for true observability, the a priori covariance matrix P_0 should not be used in the equation for computing Λ, because P_0 may artificially make the state observable when it should not be.

Acknowledgments

This material is based upon work supported under a National Science Foundation Graduate Research Fellowship. Martin W. Lo of NASA's Jet Propulsion Laboratory at the California Institute of Technology provided valuable insight and advice and this research would not have been possible without his direction.

References

[1] Chory, M. A., Homan, D. P., and LeMay, J. L., "Satellite Autonomous Navigation—Status and History," *Proceedings of the IEEE Position, Location, and Navigation Symposium*, Inst. of Electrical and Electronics Engineers, New York, 1986, pp. 110–121.

[2] Menn, M., "Autonomous Navigation for GPS via Crosslink Ranging," *Proceedings of the IEEE Position, Location, and Navigation Symposium*, Inst. of Electrical and Electronics Engineers, New York, 1986, pp. 143–146.

[3] Hicks, K. D., and Wiesel, W. E., "Autonomous Orbit Determination System for Earth Satellites," *Journal of Guidance, Control, and Dynamics*, Vol. 15, No. 3, 1992, pp. 562–566.

[4] Psiaki, M. L., "Autonomous LEO Orbit Determination from Magnetometer and Sun Sensor Data," AIAA Guidance, Navigation, and Control Conference, Boston, MA, AIAA Paper 1998-4308, 1998.

[5] Psiaki, M. L., "Autonomous Low-Earth-Orbit Determination from Magnetometer and Sun Sensor Data," *Journal of Guidance, Control, and Dynamics*, Vol. 22, No. 2, 1999, pp. 296–302.

[6] Long, A. C., Leung, D., Folta, D., and Gramling, C., "Autonomous Navigation of High-Earth Satellites Using Celestial Objects and Doppler Measurements," AIAA/AAS Astrodynamics Specialist Conference, Denver, CO, AIAA Paper 2000-3937, 2000.

[7] Psiaki, M. L., "Tests of Magnetometer/Sun-Sensor Orbit Determination Using Flight Data," *Journal of Guidance, Control, and Dynamics*, Vol. 25, No. 3, 2002, pp. 582–590.

[8] Psiaki, M. L., "Autonomous Orbit Determination for Two Spacecraft from Relative Position Measurements," *Journal of Guidance, Control, and Dynamics*, Vol. 22, No. 2, 1999, pp. 305–312.

[9] Markley, F. L., "Autonomous Navigation Using Landmark and Intersatellite Data," AIAA/AAS Astrodynamics Conference, Seattle, WA, AIAA Paper 1984-1987, 1984.

[10] Yim, J. R., Crassidis, J. L., and Junkins, J. L., "Autonomous Orbit Navigation of Two Spacecraft System Using Relative Line of Sight Measurements," AAS/AIAA Astrodynamics Specialist Conference, Maui, HA, AAS Paper 04-257, 2004.

[11] Hill, K., Lo, M. W., and Born, G. H., "Linked, Autonomous, Interplanetary Satellite Orbit Navigation (LiAISON)," AAS/AIAA Astrodynamics Specialist Conference, Lake Tahoe, CA, American Astronautical Society, Paper 05-399, 2005.

[12] Liu, Y., and Liu, L., "Orbit Determination Using Satellite-to-Satellite Tracking Data," *Chinese Journal of Astronomy and Astrophysics*, Vol. 1, No. 3, 2001, pp. 281–286.

[13] Tapley, B. D., Schutz, B. E., and Born, G. H., *Statistical Orbit Determination*, Elsevier, Burlington, MA, 2004.

[14] Farquhar, R. W., "The Control and Use of Libration-Point Satellites," NASA TR R-346, 1970.

[15] Murray, C. D., and Dermott, S. F., *Solar System Dynamics*, Cambridge Univ. Press, Cambridge, England, U.K., 1999.

[16] Howell, K., "Three-Dimensional, Periodic, 'Halo' Orbits," *Celestial Mechanics*, Vol. 32, No. 53, 1984.

[17] Howell, K., Barden, B., and Lo, M., "Application of Dynamical Systems Theory to Trajectory Design for a Libration Point Mission," *Journal of the Astronautical Sciences*, Vol. 45, No. 2, 1997, pp. 161–178.

[18] Anon., *The Merriam-Webster Dictionary*, 5th ed., Merriam-Webster Inc., Springeld, MA, 1994.

[19] Hill, K., Lo, M. W., and Born, G. H., "Liaison Navigation in the Sun–Earth–Moon Four-Body Problem," AAS/AIAA Space Flight Mechanics Conference, Tampa, FL, American Astronautical Society, Paper 06-221, 2006.

[20] Hill, K., Parker, J., Born, G. H., and Demandante, N., "A Lunar L_2 Navigation, Communication, and Gravity Mission," AIAA/AAS Astrodynamics Specialist Conference, Keystone, CO, AIAA Paper 2006-6662, 2006.

[21] Gomez, G., Howell, K., Masdemont, J., and Simo, C., "Station-keeping Strategies for Translunar Libration Point Orbits," AAS/AIAA Space Flight Mechanics Meeting, Monterey, CA, American Astronautical Society, Paper 98-168, 1998.